A Nitric Oxide-Inhibitory Ionizable Guanidine Lipid for Anti-Inflammatory mRNA Delivery in Acute Lung Injury

Xuyu Li[3, #], Jian Xu[1, 2, 3#], Kang Yang[3], Bo Zheng[4], Jun Liu[4], Qingzhe Li[5], Kun Zhang[4, *], Dejing Liu[3, *], Mao Li[1, 3*]

[1]Shenzhen Medical Academy of Research and Translation (SMART), Shenzhen 518107, China.

[2]Westlake University, Hangzhou 310030, China

[3]Institute of Chemical Biology, Shenzhen Bay Laboratory, Shenzhen, 518132, China.

[4]College of Chemistry and Materials Science, Shanghai Normal University, Shanghai 200080, China

[5]Shenzhen Salubris Pharmaceuticals Co., Ltd., Shenzhen, 518132, China.

[#]These authors contributed equally

*Corresponding author

ABSTRACT: Lipid nanoparticles (LNPs) represent the most clinically advanced platform for mRNA delivery, yet their inherent immunogenicity remains a critical barrier to therapeutic efficacy. Nitric oxide (NO) is a central effector in macrophage-driven inflammation, making it a particularly compelling molecular target for the design of anti-inflammatory LNP. Here, we screened a library of ionizable guanidine compounds and identified G9, a potent inhibitor that suppresses NO production in peritoneal M1 macrophages and reprograms macrophages toward an anti-inflammatory phenotype. Derivatization of G9 yielded G9-1, a guanidine-based ionizable lipid with an intrinsic NO-inhibitory motif, which retains full anti-inflammatory activity while enabling efficient mRNA encapsulation and preferential delivery to lung-resident cells. In a murine acute lung injury (ALI) model, G9-1 LNPs loaded with IL-10 mRNA exerted synergistic therapeutic effects, reducing inflammatory cell infiltration, suppressing pro-inflammatory cytokines and improving systemic markers of tissue injury. This work establishes NO inhibition as a design principle for anti-inflammatory ionizable lipids and introduces a new class of LNP with intrinsic immunomodulatory activity for safer mRNA therapeutics in inflammatory disorders.

Introduction

Lipid nanoparticles (LNPs) have revolutionized mRNA-based therapeutics, as exemplified by the clinical success of mRNA vaccines.[1-3] Clinically approved LNPs typically comprise four lipid components: ionizable lipids, cholesterol, helper lipids, and PEGylated lipids.[4, 5] The ionizable lipid serves as the core functional moiety, enabling pH-dependent mRNA encapsulation and endosomal escape, both prerequisites for efficient in vivo mRNA delivery and translation.[6-8] Despite their clinical success, the utility of LNPs is severely hampered by their inherent immunogenicity[9, 10]. Systemic administration of LNPs triggers a robust innate immune response characterized by pro-inflammatory cytokine secretion, which not only induces systemic inflammation and potential tissue damage but also impairs the stability and translational efficiency of the delivered mRNA.[11-13] This creates a vicious cycle: LNP-induced inflammation reduces therapeutic efficacy, necessitating higher doses, which in turn exacerbates immunogenicity.

A central driver of LNP-induced inflammation is the crosstalk between LNPs and macrophages[14, 15]. As professional phagocytes, macrophages rapidly recognize and internalize LNPs, triggering pro-inflammatory signaling cascades which leads to secretion of cytokines such as TNF-α and IL-6.[16-18] Among the downstream effectors of macrophage activation, nitric oxide (NO) plays a particularly central and self-amplifying role[19]. NO is produced from L-arginine by inducible nitric oxide synthase 2 (NOS2/iNOS), a hallmark enzyme of the pro-inflammatory M1 macrophage state.[20, 21] Critically, NO does not merely serve as a downstream effector molecule but actively sustains and amplifies the inflammatory program through multiple positive feedback mechanisms. NO stabilizes hypoxia-inducible factor 1α (HIF-1α) via S-nitrosylation, which in turn drives glycolytic reprogramming and upregulates pro-inflammatory cytokines.[22] Simultaneously, NO activates NF-κB signaling, potentiating transcriptional upregulation of iNOS itself and creating a self-reinforcing loop that sustains M1 polarization.[23] At the metabolic level, NO inhibits mitochondrial aconitase 2 (ACO2) and causing citrate accumulation that further fuels pro-inflammatory lipid mediator synthesis[24]. Together, these mechanisms establish NO as an upstream amplifier of macrophage-driven inflammation, making it a particularly compelling molecular target for anti-inflammatory intervention[25-30].

Modulating NO production therefore represents a compelling strategy to enhance LNP safety and efficacy. This is especially relevant in pulmonary inflammatory pathologies such as acute lung injury (ALI), where alveolar macrophages and interstitial macrophages are the predominant drivers of pathological inflammation.[31-41] However, despite the well-established role of NO in macrophage-driven inflammation, rational design of ionizable lipid to direct inhibit NO production has not been realized. Prior efforts to reduce LNP immunogenicity have focused on suppressing TLR-mediated innate immune sensing through lipid engineering[18, 42-45], incorporating antioxidant moieties to scavenge reactive oxygen species,[46, 47] or co-loading anti-inflammatory cargo[48, 49].

We therefore hypothesized that incorporating a NO-inhibitory motif directly into the ionizable lipid headgroup could create a new class of intrinsically anti-inflammatory LNP that suppresses macrophage NO production at the molecular level while retaining full mRNA delivery capacity. Here, we report the discovery of G9, an ionizable guanidine compound that potently inhibits NO production in primary peritoneal M1 macrophages and reprograms macrophages toward the anti-inflammatory phenotype. Derivatization of

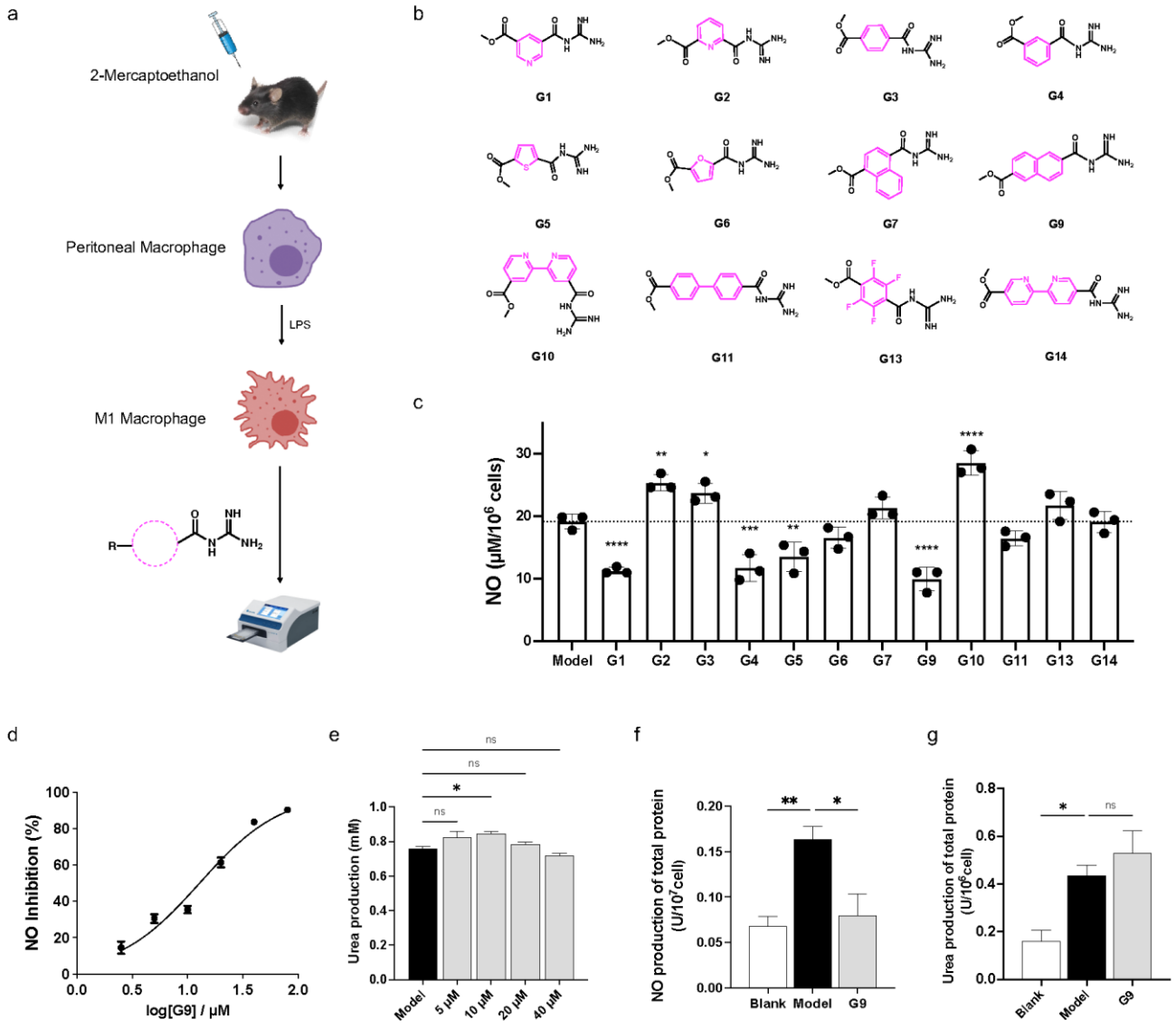

Figure 1. **G9 is a potent NO inhibitor in peritoneal macrophage.** a) Schematic of the NO inhibitor screening workflow in LPS-induced peritoneal M1 macrophages. b) Schematic representation of the acyl-guanidine compound library. c) NO production in peritoneal M1 macrophages treated with guanidine compounds at 10 μM. d) Dose-dependent inhibition of NO production by G9 in peritoneal M1 macrophages. e) Urea production in peritoneal M1 macrophages treated with G9. f) NO and Urea (g) production in total protein extracts from peritoneal M1 macrophages treated with G9.

G9 yielded G9-1, a NO-inhibitory ionizable lipid that retains anti-inflammatory activity while enabling efficient mRNA encapsulation and lung-targeted delivery. In a murine model of ALI, G9-1 LNPs loaded with IL-10 mRNA exerted synergistic therapeutic effects, demonstrating the potential of NO inhibition as a design principle for next-generation anti-inflammatory ionizable lipids

Results and Discussion

Identification of G9: a potent NO production inhibitor in peritoneal macrophage

We sought to identify a NO inhibitor with physicochemical properties compatible with integration into an ionizable lipid scaffold. Existing guanidine-derived NOS inhibitors such as L-NMMA and L-NAME carry a high pK_a and permanent positive charge, which predisposes them to non-specific protein aggregation in circulation and systemic cytotoxicity.[50-52] To overcome these limitations, we designed a series of neutral guanidine compounds in which aromatic rings are conjugated to the guanidine warhead to lower its pK_a and tune its physicochemical properties for lipid compatibility (Figure 1b).

We evaluated the NO inhibitory activity of these compounds in a lipopolysaccharide (LPS)-induced peritoneal M1 macrophage model using per-cell NO production as a direct readout (Figure 1a). LPS is a potent inducer of M1 polarization and NO expression. The results showed that several compounds blocked M1 macrophage NO production at 10 μM. Notably, G9 exhibited exceptional efficacy, reducing NO production by 50% compared to untreated controls (Figure 1c). Cellular assays revealed a concentration-dependent inhibitory effect of G9, with an IC_{50} of ~12.6 μM in

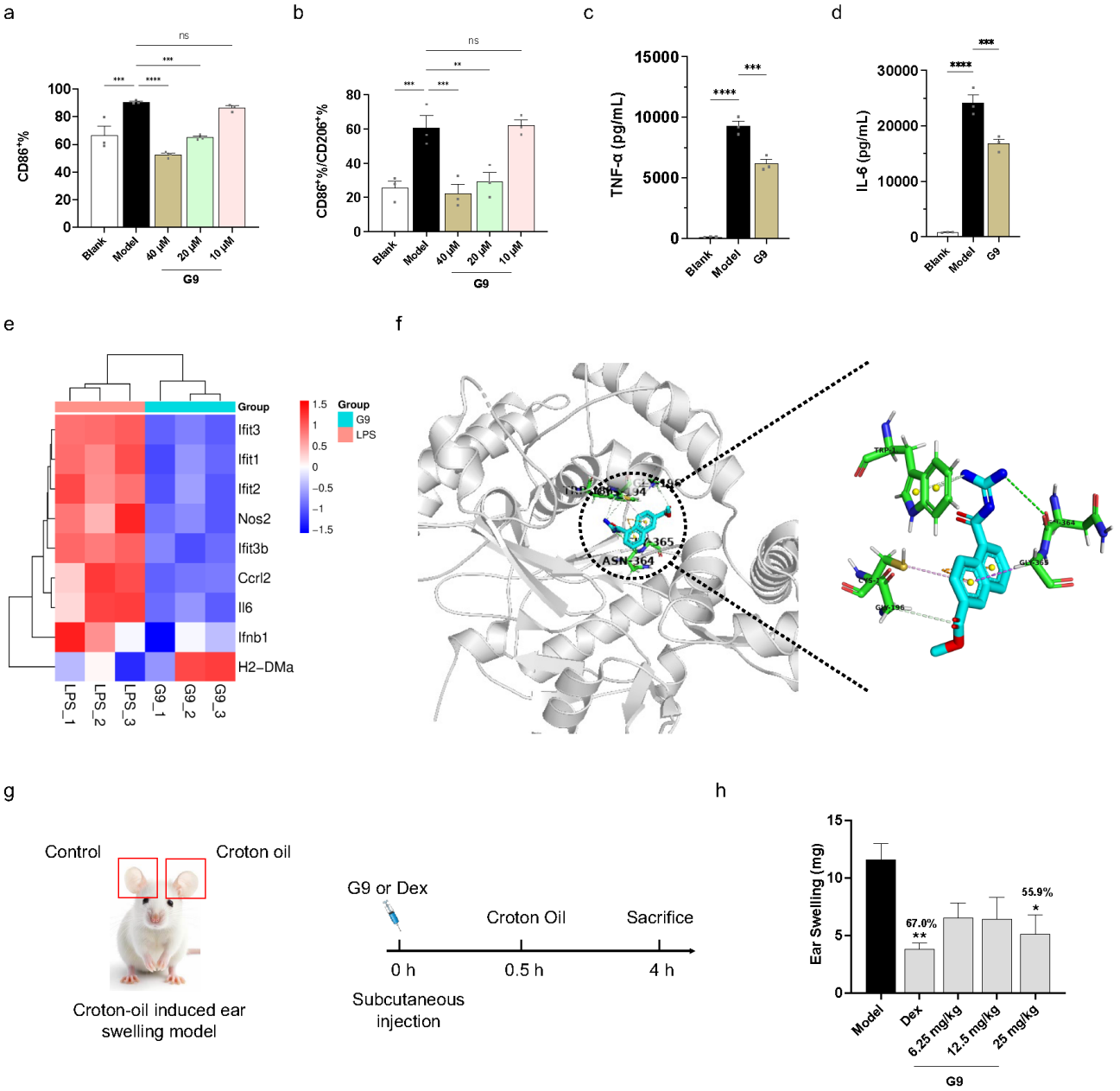

Figure 2. **G9 reprograms macrophage polarization towards the anti-inflammation phenotype**. Surface marker expression (a: CD86%; b: CD86%/CD206% ratio) in peritoneal M1 macrophages treated with G9. c-d) Secretion of TNF-α (c) and IL-6 (d) by peritoneal M1 macrophages treated with G9. e) RNA-seq analysis of G9 and LPS-treated RAW264.7 macrophages. f) Molecular docking of G9 within the NOS2 active site. g) Schematic representation of the ear edema model of acute cutaneous inflammation and the treatment strategy. h) Ear swelling inhibition of G9 or Dex-treated mice.

LPS-induced peritoneal M1 macrophages (Figure 1d). In LPS-stimulated RAW264.7 macrophages, the IC_{50} of G9 was determined to be 20.6 μM, superior than that of L-NMMA (IC_{50}: 30–40 μM)[53], a well-characterized arginine-derived NO inhibitor (Supp Info. Figure S1). Importantly, no cytotoxicity was observed for G9 in macrophage cells at concentrations up to 500 μM, confirming its safety profile (Supp Info. Figure S2).

Arginine metabolism in macrophages can proceed via two competing pathways: the NOS-dependent pathway, which produces NO, and the ARG1-dependent pathway, which degrades arginine to urea.[54, 55] Inhibition of NO activity by G9 would be expected to increase substrate availability for ARG1, potentially elevating urea production. Nevertheless, G9-treated macrophages showed only a modest trend toward increased urea production (Figure 1e). To further characterize G9's mechanism of action, we measured both NO and urea production from total protein extracts of peritoneal M1 macrophages. G9 significantly inhibited total NO production (Figure 1f) while leaving urea production unaffected (Figure 1g). Consistent with this selectivity, G9 also inhibited recombinant NOS2 activity in a cell-free assay, suggesting that G9 might act as a direct NOS2 inhibitor that blocks NO production (Supp Info. Figure S3).

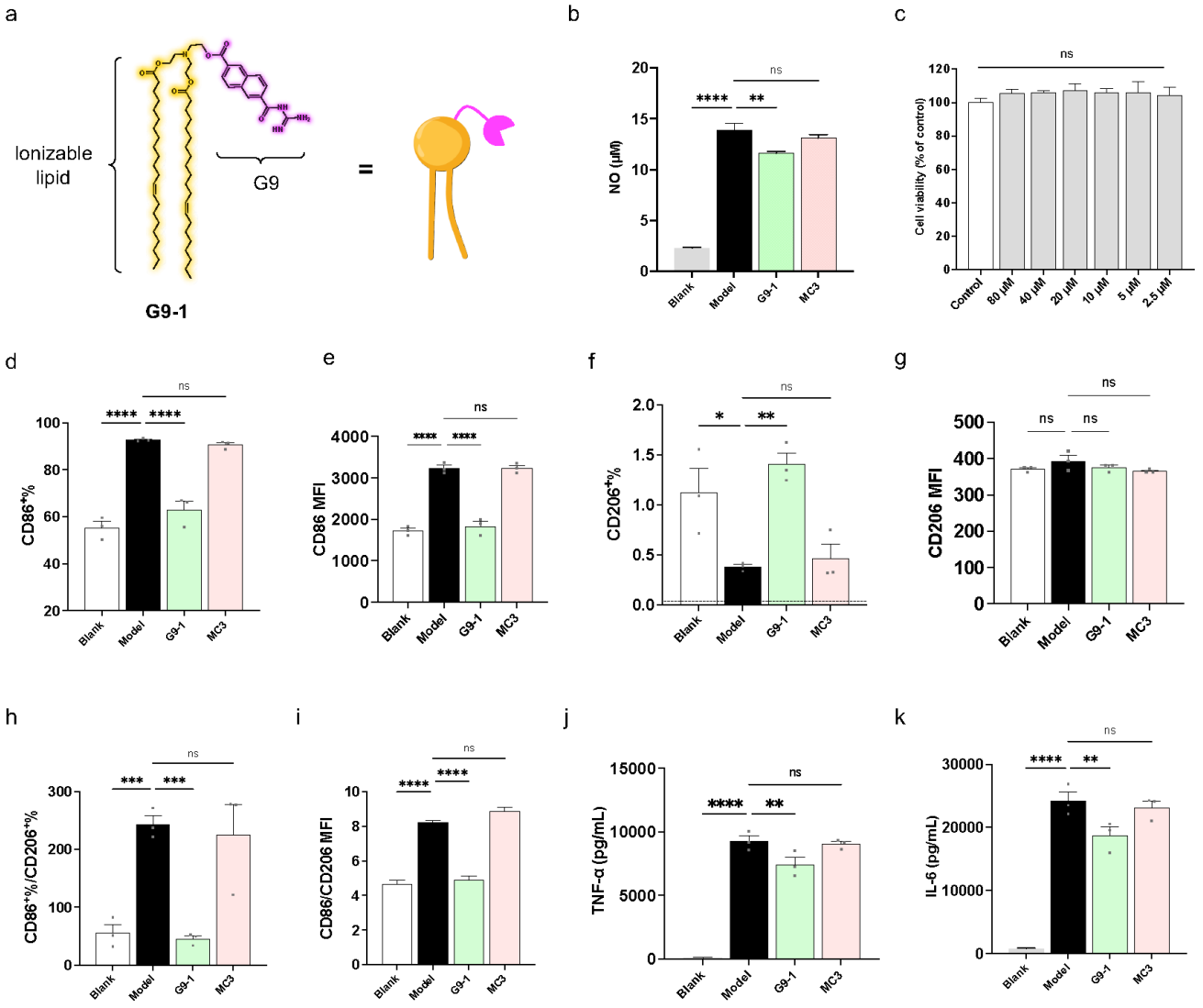

Figure 3. **G9-1 is a NO-inhibitory ionizable lipid and reprograms macrophage polarization**. a) Chemical structure of G9-1. b) NO production in LPS-induced peritoneal M1 macro-phages treated with G9-1 and MC3 lipids. c) Cell viability of peritoneal M1 macro-phages treated with G9-1. d-i) Surface marker expression (d: CD86%; e: CD86 mean fluorescence intensity (MFI); f: CD206%; g: CD206 MFI; h: CD86/CD206%; i: CD86/CD206 MFI) in peritoneal M1 macrophages treated with G9-1 and MC3 lipids. j-k) Secretion of TNF-α (j) and IL-6 (k) by peritoneal M1 macrophages treated with G9-1 or MC3 lipid.

G9 reprograms macrophage polarization and inhibits proinflammatory cytokine secretion

We next asked whether NO inhibition by G9 is sufficient to drive macrophage reprogramming toward the anti-inflammatory phenotype. G9 dose-dependently decreased CD86 expression in peritoneal macrophages (Figure 2a and Supp Info. Figure S4), significantly shifting the CD86/CD206 ratio (Figure 2b), a surrogate for M1/M2 polarization. Correspondingly, G9 significantly inhibited the secretion of pro-inflammatory cytokines TNF-α and IL-6 (Figure 2c–d), demonstrating that NO inhibition is sufficient to broadly suppress the macrophage inflammatory program.

Transcriptomic analysis confirmed that G9 treatment broadly reversed the pro-inflammatory transcriptional program triggered by LPS (Figure 2e). G9 robustly downregulated interferon-stimulated genes (ISGs) including Ifit1/2/3 and Ifit3b, as well as the type I interferon Ifnb1, indicating suppression of the IFN-mediated inflammatory cascade. Concurrently, G9 markedly reduced expression of Il6 and Nos2, consistent with the self-reinforcing anti-inflammatory effect of NO inhibition. Notably, G9 enhanced expression of H2-DMa, an MHC class II molecule critical for antigen presentation, suggesting that G9 may function as a selective immunomodulator that dampens pathological innate inflammation while preserving adaptive immune responses.

To elucidate the molecular mechanism underlying G9's NO inhibitory activity, we performed molecular docking studies with NOS2. G9 exhibits a tight binding to NOS2 with multiple non-covalent interactions (Figure 2f). The naphthalene group in G9 formed CH-π interactions with the α-CH_2 of Gly365, the guanidine motif engaged in cation-π interactions with the indole ring of Trp188, and the guanidine

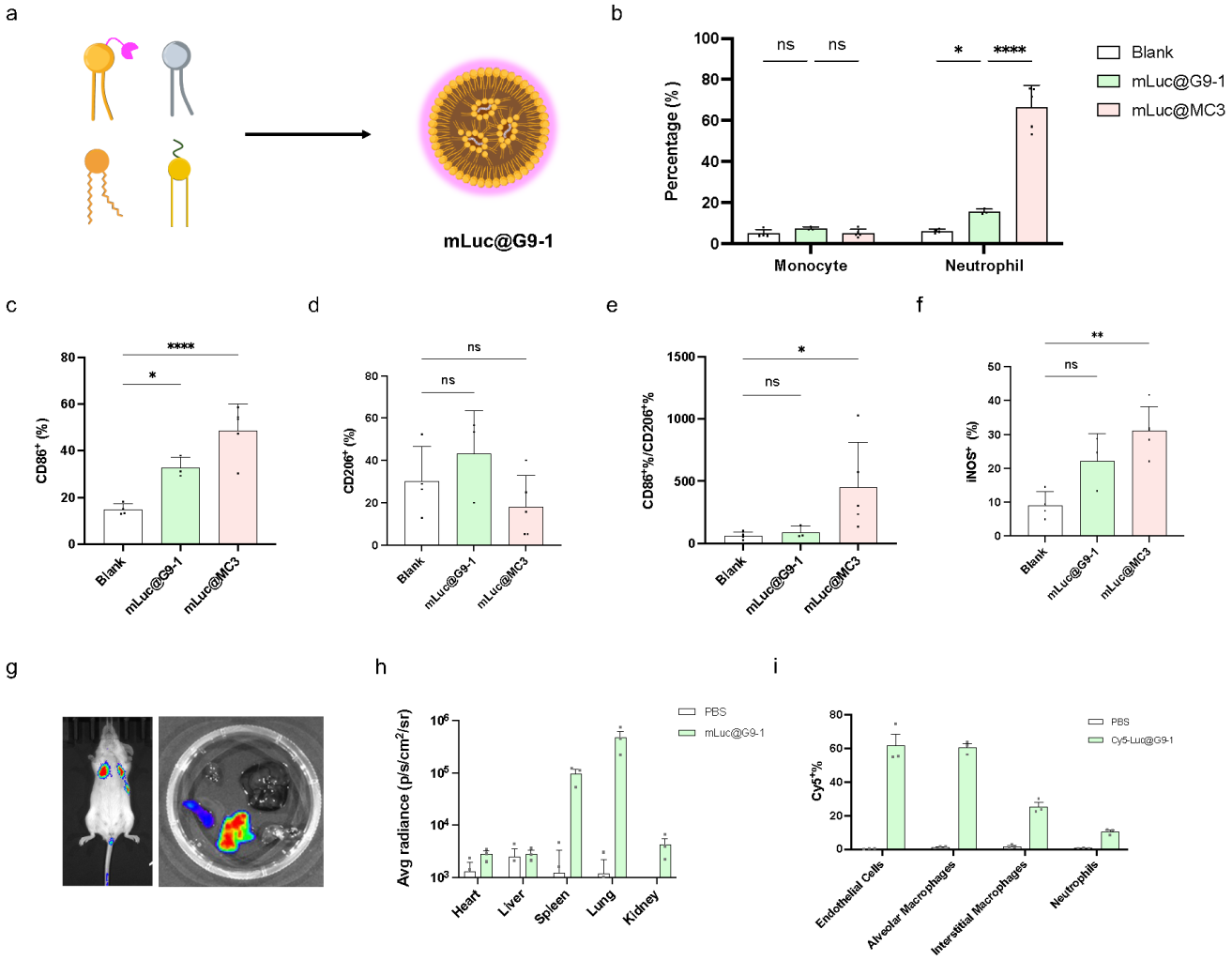

Figure 4. G9-1 LNP inhibits inflammatory responses and enables lung-targeted mRNA delivery. a) Schematic representation of G9-1 LNP. b) Percentage of monocytes and neutrophils in peripheral blood of mice treated with G9-1, MC3 and PBS groups. c–f) Surface marker expression (c: CD86%; d: CD206%; e: CD86/CD206%; f: iNOS) in blood monocytes of mice. g) Bioluminescence IVIS imaging of whole body and isolated organs from mice administered with mLuc@G9-1(i.v.). h) Average radiance in isolated organs from mLuc@G9-1 treated mice. j) Flow cytometry analysis of $Cy5^+$ cell populations in the lung.

moiety formed hydrogen bonds with Asn364. However, compound G7, which contains a naphthalene group at a different substitution position, did not alter macrophage NO production (Figure 1c), highlighting the structural specificity of G9's inhibitory effect.

To further validate G9's anti-inflammatory efficacy *in vivo*, we employed a croton oil-induced murine ear edema model of acute cutaneous inflammation. Subcutaneous administration of G9 significantly alleviated ear edema in a dose-dependent manner, with efficacy comparable to dexamethasone (Dex), a clinically approved anti-inflammatory corticosteroid. Collectively, these results establish G9 as a potent inhibitor that suppresses macrophage NO production, drives M1-to-M2 reprogramming and exerts anti-inflammatory effects both *in vitro* and *in vivo* (Figure 2g-h).

G9-1: A NO-Inhibitory ionizable lipid that reprograms macrophage polarization

Having validated G9 as a potent NO inhibitor with *in vivo* anti-inflammatory activity, we sought to translate this activity into an ionizable lipid scaffold. The key design feature is to conjugate the NO-inhibitory headgroup of G9 to a lipid tail in a manner that: (1) preserves NO inhibitory activity, (2) confers the pH-dependent ionization behavior required for mRNA encapsulation and (3) enables self-assembly into LNPs with favorable physicochemical properties.[33]

We thus designed and synthesized G9-1, a derivative of G9 in which the acyl-guanidine motif is conjugated to the lipid headgroup (Figure 3a). To confirm that G9-1 retains NO inhibitory activity, we treated LPS-induced peritoneal M1 macrophages with G9-1 and measured NO production. G9-1 significantly inhibited NO production, albeit with reduced potency compared to G9 (Figure 3b). In LPS-induced RAW macrophages, the IC_{50} of G9-1 for NO inhibition was determined to be ~45 μM (Supp. Info. Figure S5). Moreover, G9-1 exhibited negligible cytotoxicity to peritoneal macrophages, suggesting that the NO-inhibition effect is not originated from decreased cell proliferation (Figure 3c). Critically, G9-1 treatment decreased both CD86 expression and intensity (Figure 3d-e), while increasing the expression and intensity of CD206 (Figure 3f-g),

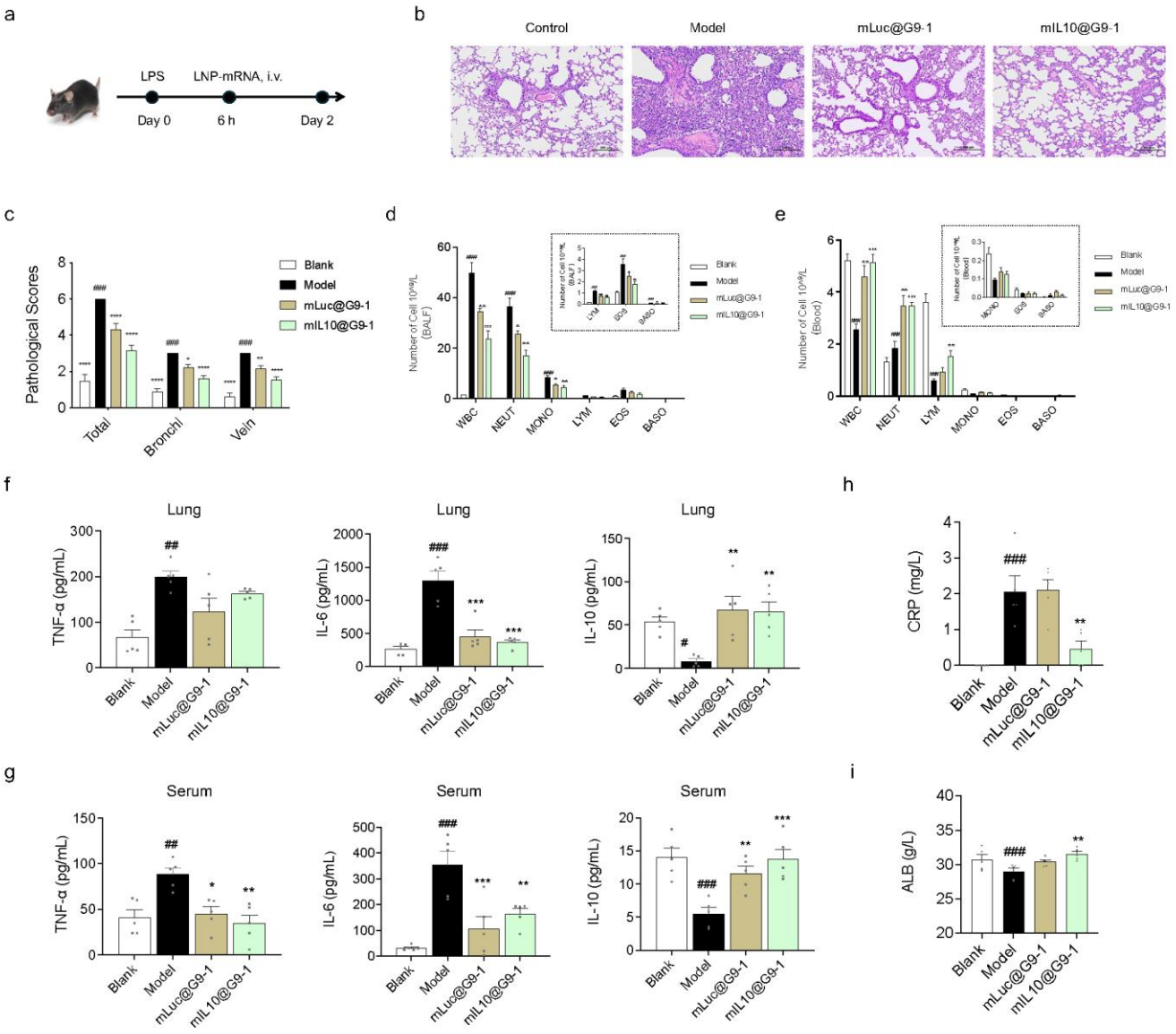

Figure 5. G9-1@IL-10 mRNA exerts synergistic therapeutic effects in a murine ALI model. a) Schematic of the LPS-induced ALI model and treatment strategy. b–c) Representative H&E-stained lung sections (b) and quantitative inflammation scores (c) of the mice after the treatment (n=3). d–e) Five-part leukocyte differential counts in BALF (d) and peripheral blood (e) of the mice after the treatment (n=5). f–g) Cytokine levels (TNF-α, IL-6, IL-10) in the lung (f) and serum (g) after the treatment (n=5). h–i) Serum CRP (h) and albumin (ALB) (i) concentrations after treatment.

significantly shifting the M1/M2 ratio in a manner that mirrored the effect of G9 (Figure 3h-i). In sharp contrast, the clinically approved DLin-MC3-DMA (MC3) lipid did not alter the M1/M2 ratio in macrophages, confirming that the anti-inflammatory effect of G9-1 is specifically mediated by the NO-inhibitory property. G9-1 also significantly inhibited secretion of TNF-α and IL-6 in primary macrophages (Figure 3j-k), further validating its anti-inflammatory activity.

G9-1 LNP inhibits inflammatory response in vivo and enables lung-targeted mRNA delivery

We next formulated LNPs using G9-1 as the ionizable lipid, alongside DOPE, DOTAP and DMG-PEG 2000. As previously demonstrated for ionizable guanidine-based LNPs, cholesterol was omitted from the formulation.[56] The molar ratio of components was set to 50:2.5:26.5:0.5 (G9-1: DOPE: DOTAP: DMG-PEG). Dynamic light scattering (DLS) analysis revealed a mean particle size of ~135 nm and a zeta potential of ~+5 mV at neutral pH (Supp Info. Figure S7). G9-1 LNPs exhibited high encapsulation efficiency (>80%) for IL-10 mRNA (Supp Info. Figure S8), confirming that the NO-inhibitory motif does not compromise mRNA binding capacity.

We evaluated the inflammatory response of G9-1 LNPs encapsulating Luc mRNA (mLuc@G9-1) and compared it to that of the standard MC3 LNP (mLuc@MC3). Intravenous administration of LNPs has been shown to trigger acute inflammatory responses characterized by rapid changes in peripheral blood immune cell composition, particularly neutrophils and monocytes.[57, 58] As shown in Figure 4b, administration of mLuc@MC3 led to a more than 10-fold elevation in the percentage of neutrophils in peripheral blood

compared to the PBS group, indicating a severe inflammatory response. In sharp contrast, mLuc@G9-1 induced only a mild increase (~2.5-fold) in neutrophils, highlighting its anti-inflammatory property. Examination of monocyte surface markers further confirmed the superior anti-inflammatory profile of G9-1 LNPs: CD86 expression was markedly lower and the M1/M2 ratio remained comparable to the PBS group (Figure 4c–e and Supp Info. Figure S9-10), whereas MC3 LNP treatment led to a significant increase in M1 markers and M1/M2 ratios. Furthermore, NOS2 expression in peripheral blood monocytes was not elevated in the mLuc@G9-1 group, in contrast to the mLuc@MC3 group (Figure 4f), directly confirming the NO-inhibitory activity of the G9-1 lipid in vivo.

To evaluate the *in vivo* delivery performances, mLuc@G9-1 were administered intravenously to Balb/c mice. IVIS imaging revealed predominant expression in the lung with secondary expression in the spleen (Figure 4g-h). The cell-type specificity of G9-1 in the lung was then determined using Cy5-labeled mRNA (Cy5-Luc) intravenously by flow cytometry on dissociated lung cells. G9-1 LNP delivered mRNA primarily to lung endothelial cells (61.7%) and alveolar macrophages (60.8%), cell types centrally involved in ALI pathogenesis, followed by interstitial macrophages (25.4%) and neutrophils (Figure 4i and Supp Info. Figure S11-12).

Together, these findings establish G9-1 as an ionizable lipid that combines two functions in a single molecular scaffold: intrinsic anti-inflammatory activity via NO inhibition, and efficient mRNA delivery with preferential targeting to pulmonary vascular endothelial cells and alveolar macrophages. This dual functionality makes G9-1 ideally suited for the treatment of pulmonary inflammatory disorders.

G9-1 LNPs exert synergistic therapeutic effects in a murine model of ALI

Acute lung injury (ALI) is a life-threatening respiratory disorder characterized by macrophage-dominated acute pulmonary inflammation, leading to severe damage to the pulmonary vascular endothelium and alveolar epithelium, and ultimately respiratory failure.[20,21] Given that alveolar macrophages are the primary drivers of ALI pathogenesis, and that NO is a key mediator of macrophage-driven tissue damage,[36] we reasoned that a NO-inhibitory ionizable lipid would be particularly well-suited for ALI therapy. We therefore investigated whether G9-1 LNP loaded with IL-10 mRNA, a potent anti-inflammatory cytokine that inhibits macrophage activation,[21] could exert therapeutic effects in an LPS-induced murine ALI model.

We established the ALI model by intratracheal instillation of LPS into Balb/c mice. Subsequently, mice were treated intravenously with: (1) PBS, (2) G9-1 LNPs encapsulating luciferase mRNA (mLuc@G9-1), or (3) G9-1 LNPs encapsulating IL-10 mRNA (mIL10@G9-1). This design allowed us to dissect the intrinsic anti-inflammatory contribution of the G9-1 lipid from the combined effect of the lipid and the therapeutic IL-10 mRNA payload (Figure 5a).

Histopathological analysis of lung tissue via H&E staining revealed that LPS-induced ALI caused severe lung damage, including alveolar wall thickening, inflammatory cell infiltration, and alveolar hemorrhage (Figure 5b). mLuc@G9-1 treatment significantly alleviated these pathological changes, demonstrating that the NO-inhibitory activity of the G9-1 lipid alone is sufficient to confer meaningful protection against ALI-associated lung damage. mIL10@G9-1 treatment exerted an even stronger protective effect, with lung tissue morphology approaching that of healthy controls. Inflammatory scoring confirmed these observations: mIL10@G9-1-treated mice had significantly lower bronchial and vascular inflammation scores compared to both the ALI model and mLuc@G9-1 groups (Figure 5c).

To quantify the inflammatory response, we analyzed the cellular composition of bronchoalveolar lavage fluid (BALF). LPS-induced ALI led to a significant increase in total leukocytes, neutrophils, monocytes, lymphocytes, and basophils in BALF (Figure 5d). mLuc@G9-1 treatment significantly reduced the number of these inflammatory cells, demonstrating that NO inhibition by the G9-1 lipid is sufficient to suppress inflammatory cell recruitment to the lung, independent of any mRNA payload. mIL10@G9-1 treatment further suppressed BALF leukocytes, neutrophils, and basophils, demonstrating a synergistic effect between NO inhibition by the G9-1 lipid and anti-inflammatory signaling by the delivered IL-10 mRNA. Concurrently, peripheral blood analysis revealed an increase in circulating leukocytes and neutrophils in G9-1-treated mice (Figure 5e), consistent with inhibition of inflammatory cell migration into the lung, a critical step in ALI pathogenesis.

We next measured pro-inflammatory and anti-inflammatory cytokine levels in both lung and serum. In the lung, LPS-induced ALI significantly elevated TNF-α and IL-6 levels while reducing IL-10 (Figure 5f). mLuc@G9-1 treatment significantly reduced IL-6 levels, consistent with its NO-inhibitory and anti-inflammatory properties. mIL-10@G9-1 treatment markedly reduced both TNF-α and IL-6 levels and substantially elevated IL-10 in the lung, confirming that the delivered IL-10 mRNA is efficiently translated into functional protein and amplifies the anti-inflammatory effect of the G9-1 lipid. Serum cytokine profiles mirrored these trends, with mIL-10@G9-1 treatment significantly reducing systemic TNF-α and IL-6 levels and increasing IL-10 level (Figure 5g).

To assess systemic inflammation and organ function, we measured serum CRP (a marker of acute-phase inflammation) and albumin (ALB, a liver-derived protein whose levels decline during inflammation). LPS-induced ALI increased serum CRP and decreased serum ALB (Figure 5h-i). mIL10@G9-1 treatment markedly suppressed serum CRP and elevated serum ALB, indicating reduced systemic inflammation and improved liver function. Body weight analysis further confirmed the therapeutic benefit: ALI model mice exhibited 5–7% weight loss on days 1–2 post-LPS, whereas mIL10@G9-1 treatment markedly attenuated this weight reduction (Supp Info. Figure S13).

Collectively, these data demonstrate that the NO-inhibitory activity of the G9-1 lipid confers significant intrinsic anti-inflammatory efficacy in a murine ALI model. When combined with IL-10 mRNA, mIL10@G9-1 achieves synergistic therapeutic effects through complementary mechanisms: direct NO inhibition by the lipid suppresses macrophage activation and inflammatory cell recruitment,

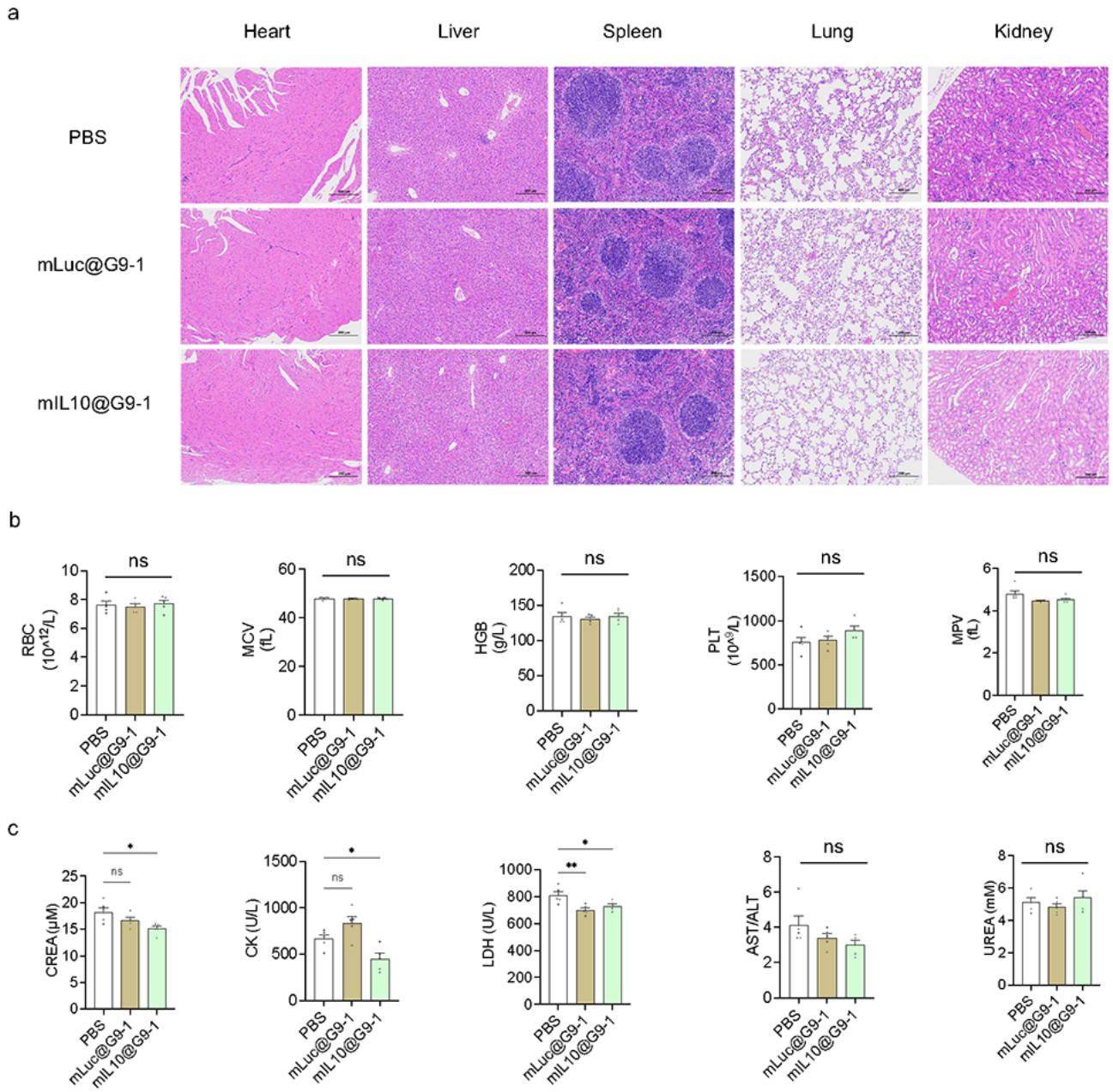

Figure 6. G9-1 exhibits excellent safety profile in Balb/c mice. a) Representative H&E-staining of mice organs. b) Erythrocyte parameters analysis of the mice after the treatment (n=5). c) Serum biochemical index of the mice (n=5).

while the delivered IL-10 mRNA amplifies anti-inflammatory signaling at the transcriptional level.

G9-1 LNP exhibits excellent safety profile

To further evaluate the biosafety of G9-1 LNPs, we administered them intravenously to healthy Balb/c mice (mLuc@G9-1 or mIL10@G9-1) and analyzed major organs (heart, liver, spleen, lung, kidney) via H&E staining 24 hours post-administration. No pathological damage such as necrosis, inflammation, or fibrosis was observed in any organ, confirming the safety of G9-1 (Figure 6a).

Erythrocyte parameters analysis revealed no significant changes in G9-1 treated mice compared to the control group (Figure 6b). Serum biochemical testing showed no marked changes in markers of liver function (AST/ALT) and kidney function (urea). Notably, both mLuc@G9-1 and mIL10@G9-1 significantly reduced serum levels of creatinine (Crea), creatine kinase (CK), and lactate dehydrogenase (LDH), markers of kidney damage, muscle damage, and general tissue injury, consistent with the systemic anti-inflammatory activity of the G9-1 lipid and its favorable safety profile (Figure 6c).

Summary and Outlook

In summary, we establish NO inhibition as a rational and actionable design principle for anti-inflammatory ionizable lipids. NO is a central amplifier of macrophage-driven inflammation: produced by NOS2 in response to LPS and other danger signals, NO sustains M1 polarization through a self-reinforcing loop and promotes pro-inflammatory

cytokine production. By identifying G9 as a potent NO inhibitor and engineering it into the G9-1 ionizable lipid scaffold, we demonstrate that NO-inhibitory activity can be embedded directly into the lipid chemistry without compromising mRNA delivery performance. The synergistic therapeutic effect of G9-1 LNPs loaded with IL-10 mRNA in a murine ALI model further demonstrates the potential of combining intrinsic lipid anti-inflammatory activity with therapeutic mRNA payloads. G9-1 LNP alone exerted significant anti-inflammatory efficacy attributable to NO inhibition, while co-delivery of IL-10 mRNA further amplified these effects through complementary mechanisms operating at different levels of the inflammatory cascade. This synergistic framework represents a broadly applicable strategy for inflammatory disorders driven by macrophage activity. Future studies directly quantifying NO production and NOS2 enzymatic activity in LNP-treated macrophages *in vivo,* and extending this design principle to other lipid architectures will further advance the development of next-generation anti-inflammatory mRNA delivery systems.

The NO-inhibitory ionizable guanidine headgroup can be conjugated to a lipid tail without sacrificing mRNA encapsulation efficiency or delivery performance. This design principle could be extended to other immunomodulatory targets relevant to macrophage activation (e.g., NF-κB pathway inhibitors, NLRP3 inflammasome inhibitors, or metabolic enzyme inhibitors), opening a new avenue for the engineering of next-generation ionizable lipids with programmable anti-inflammatory profiles.

In conclusion, our work introduces NO inhibition as a viable design principle for anti-inflammatory ionizable lipids, and establishes G9-1 as a NO-inhibitory ionizable lipid for safer and more effective LNP-based mRNA therapeutics. By embedding immunomodulatory function directly into the lipid chemistry, we provide a new framework for addressing LNP immunogenicity at its molecular source, one that is mechanistically grounded and compatible with existing mRNA delivery platforms.

Methods

Cell lines

The RAW264.7 cells (mouse mononuclear macrophages Cells) were maintained in DMEM with 10% FBS, penicillin (100 U/ml) and streptomycin (100 μg/ml) at 37°C in a humidified atmosphere with 5% CO_2.

Animal studies

Female Balb/c mice (6–8 weeks, 18–20 g), male Kunming mice, and C57BL/6J male mice (6–8 weeks, 18–20 g) were housed under standard conditions with controlled temperature and humidity in a 12 h light/dark cycle (GemPharmatech Co., Ltd, Nanjing, China). All animal experiments were approved by the Institutional Animal Care and Use Committee of Shenzhen Bay Laboratory (AELM202301, AELM202401).

Primary peritoneal macrophage isolation, culture, stimulation and analysis

Primary murine peritoneal macrophages were isolated from C57BL/6J male mice by intraperitoneal injection of 3% thioglycollate medium and cultured. Cells were isolated and plated into 96-well plates (2×10^5 cells/well, Costar, USA). For anti-inflammatory evaluation, macrophages were pretreated with the indicated compounds for 1 hour at 37°C, then stimulated with 1 μg/mL LPS for 24 h to induce NO production. Cell supernatant (100 μL) was mixed with 100 μL Griess reagent (equal volumes of 0.1% N-1-naphthylethylenediamine and 1% sulfanilamide) and incubated for 10 min at room temperature in the dark. Absorbance at 570 nm was measured using a microplate reader (Agilent BioTek Synergy H1) and NO content was calculated from a sodium nitrite standard curve.

Cell viability was assessed using the CCK-8 assay. Briefly, following treatment and LPS stimulation, 100 μL of cell supernatants were collected. 10 μL CCK-8 solution (APExBIO, Houston, USA) was added to each well, and the plates were incubated at 37°C for 30 min. Absorbance at 450 nm was measured using a microplate reader.

The concentrations of cytokines (TNF-α, IL-6, IL-10) and urea in macrophage cell supernatants (treated with 10 μM compounds, stimulated with 1 μg/mL LPS) were measured using ELISA kits (Biolegend, California, USA) according to the manufacturer's protocols.

Protein markers on the surface of macrophages cells was assessed using FITC anti-mouse F4/80 antibody, APC anti-mouse CD86 antibody, PE anti-mouse CD206/MMR antibody (Elabscience Biotechnology Co. Ltd. Wuhan, China). Each sample (2×10^5 cells) of cells was incubated with 100 μL of PBS containing 1 μL staining solutions above ice box in dark for 30 min. After centrifugation, blank control and single staining EP tubes contained 200 μL PBS were prepared, then 10^5 macrophages cells were analyzed by flow cytometry.

RNA-seq analysis

RAW264.7 was treated with G9 or LPS for 24 h, followed by total RNA extraction to analyze the expression of inflammation-related genes. Total RNA of different treatments was extracted using Trizol reagent kit (Invitrogen, Carlsbad, CA, USA) according to the manufacturer's protocol. The extracted RNA was then subjected to high-throughput sequencing. Differential expression analysis was performed, and the resulting data were mapped to the Kyoto Encyclopedia of Genes and Genomes (KEGG) database to identify significantly enriched pathways related to the inflammatory response.

Molecular docking

The crystal structure of inducible nitric oxide synthase was obtained from the Protein Data Bank (PDB ID: 3NW2). Protein preparation included removal of water molecules and irrelevant heteroatoms, addition of hydrogen atoms, and assignment of protonation states under physiological conditions. The binding pocket was defined based on the co-crystallized ligand MPW in the 3NW2 structure. The docking grid was centered on the MPW binding site, ensuring coverage of the native ligand-binding region. Ligands were prepared by generating 3D conformations and minimizing their geometry prior to docking. Molecular docking was performed using AutoDock Vina (or equivalent software), generating multiple binding poses for each ligand. The top-ranked poses were selected based on docking scores. To further improve prediction reliability, docking results were evaluated using the deep learning-based model DeepMice. Final candidate selection was based on a combination of

docking scores, DeepMice predictions, and binding mode analysis. Protein–ligand interactions, including hydrogen bonds and hydrophobic contacts, were analyzed using PyMOL.

Croton oil-induced ear edema

Male Kunming mice were randomly divided into groups of 5. For the dose–response experiment, mice received subcutaneous (s.c.) injection of G9 (6.25, 12.5, or 25 mg/kg) or dexamethasone (Dex, 1 mg/kg) as a positive control; vehicle-treated mice served as the negative control. Thirty minutes after injection, acute cutaneous inflammation was induced by topical application of 50 μL of 4% (v/v) croton oil solution to the left ear surface; the right ear was left untreated as an internal control. Four hours later, mice were euthanized under anesthesia, and 8 mm diameter ear punches were collected from both ears. The degree of ear edema was quantified as the weight difference between the left (treated) and right (untreated) ear.

Preparation for LNP

G9-1 lipid was dissolved in DMSO (50 mg/ml), DOPE and DMG-PEG2000 were dissolved in ethanol (10 mg/mL), DOTAP were dissolved in ethanol (50 mg/ml). G9-1 LNPs were formulated with G9-1, DOPE, DMG-PEG2000 and DOTAP in a molar ratio of 50:2.5:0.5:26.5. MC3 LNPs were fixed with MC3 lipids, DSPC, cholesterol, DMG-PEG 2000 in a molar ratio of 50:10:38.5:1.5. The lipid components and Luc-mRNA solutions were mixed according to the indicated formulations (total lipid: mRNA = 1:3) using pipettes (up and down rapidly for 60 s) or microfluidic mixing for *in vitro* or *in vivo* studies. After microfluidic mixing, LNPs were dialyzed into PBS with Slide-A-Lyzer™ dialysis cassettes (10K MWCO, Thermofisher).

Dynamic light scattering

LNP was diluted to 0.5mg/ml in PBS and tested for particle size and zeta potential using dynamic light scattering (Zetasizer Pro, Malvern Panalytical). Each sample was examined three times. Diameters are reported as intensity means peak average.

Analysis of peripheral blood immune cells

Peripheral blood was collected from the retro-orbital sinus of female C57BL/6J mice at 24h post-administration (i.v.) of mLuc@MC3 or mLuc@G9-1 LNPs (0.5 mg/kg). The blood samples were anticoagulated with 5 mM EDTA. 50 μL of whole blood was resuspended in FACS buffer (PBS supplemented with 2% FBS) and stained with fluorophore-conjugated surface antibodies: Alexa Flour 700 anti-mouse CD45, FITC anti-mouse CD11b, BV510 anti-mouse Gr-1, BV650 anti-mouse CD86, and PE anti-mouse CD206/MMR.

Following a 30 min incubation at room temperature in the dark, the cells were fixed for 15 min and washed with 3 mL of PBS. For intracellular staining, the cells were then incubated for 15 min with PE-Cy7 anti-mouse iNOS antibody (diluted 1:100 in permeabilization buffer). The permeabilization step simultaneously facilitated the lysis of red blood cells. After incubation, the samples were washed twice and resuspended in 200 μL of PBS. Unstained and single-stained controls were prepared concurrently to establish compensation matrices. Data acquisition was subsequently performed on a flow cytometer.

In vivo mRNA delivery

Female Balb/c mice (n = 3) were treated with Luc mRNA-loaded LNPs at an mRNA dose of 0.4 mg/kg (i.v.). After 3 h, mice were anesthetized with isoflurane and injected intraperitoneally with 200 μL D-Luciferin (potassium salt, 30 mg/mL). After 4 minutes, mice were imaged using an IVIS Spectrum (PerkinElmer), and organs (heart, liver, spleen, lung, kidney) were immediately excised and imaged. Average radiance in mice and isolated organs was quantified using Living Image software.

Cy5-Luc mRNA (0.4 mg/kg, i.v.) was used to examine the biodistribution of LNPs in the lung tissues. After 3h, the lungs of mice were harvested and digested using 2 mg/mL collagenase IV and 0.1 mg/mL DNAse, followed by filtration through a 200-mesh strainer and centrifuged (300g, 5min) at 4°C. Using red blood cell lysis buffer and PBS buffer to obtain single cell suspension. Each sample (2×10^5 cells) of cells was incubated with 100 μL of PBS containing 0.2 μL staining solutions above ice box in dark for 30 min, containing Alexa Flour 700 anti-mouse CD45 antibody (immune cells), BV 605 anti-mouse CD31 (endothelial cells), BV 786 anti-mouse CD326 (epithelial cells), PE/cyanine7 anti-mouse CD3 antibody (T cells), BV 421 anti-mouse CD19 (B cells), PE/cy5 anti-mouse F4/80 antibody (Macrophages), FITC anti-mouse CD11b antibody (Neutrophil), PerCP/cy5.5 anti-mouse CD11c antibody (DCs).

LPS-induced mice acute lung injury

Female Balb/c mice were randomly divided into groups. On day 0, all mice except the PBS control group received intratracheal instillation of LPS (120 μg in 50 μL PBS). Six hours after LPS instillation, mice were administered (i.v.) with PBS, mLuc@G9-1(0.3 mg/kg) and mIL10@G9-1(0.3 mg/kg). Body weight was recorded daily. On day 2 (48 h after LPS instillation), mice were euthanized and lung tissue, BALF, and blood were collected for further analysis.

Lung tissue was fixed in 10% (v/v) formalin solution and Paraffin-embedded, which was subsequently sliced in 4 μm thickness and stained with hematoxylin-eosin (H&E) solution to observe pathological changes and analysis inflammatory cell infiltration as described previously. A 4-point scale was used, and the assessment was performed in a single-blind fashion: 0 point: no inflammatory cell infiltration in bronchus and vessels; 1 point: occasional cuff-like inflammatory cell infiltration; 2 points:1–5 layer(s) of inflammatory cells infiltrated in most of bronchus and vessels; 3 points: inflammatory cells greater than 5 layers infiltrated in most of bronchus and vessels. Total lung injury score was the sum of bronchus and vessel score, each slice was observed 5 fields of view, and their average of bronchus and vessel score was taken.

BALF was collected by intratracheal instillation with 700 μL PBS triply. After centrifugation, the supernatant was stored to test the concentration of TNF-α, IL-6 and IL-10 by ELISA kits (Biolegend, California, USA), and the number of cells in the BALF and blood were counted via a hemocytometer (Mindray BC-5000 vet, Shenzhen, China). The protein concentration of BALF was tested by BCA protein assay kit (Solarbio science & technology Co., Ltd, Beijing, China). The CRP and ALB concentration of serum was tested by biochemical analyzer (Mindray BS-240 Vet, Shenzhen, China).

Safety assessment

Female Balb/c mice were divided into groups randomly for evaluating potential LNPs-induced toxicity. Mice were administered (i.v.) with mLuc@G9-1(0.3 mg/kg) and mIL10@G9-1(0.3 mg/kg). After 24h, animals were harvested and collected organs, blood and serum for further measurement, including histopathological examination of major organs (heart, liver, spleen, lungs, and kidneys) by H&E staining; complete blood count analysis measuring five-part leukocyte differentials (total leukocytes, neutrophils, monocytes/macrophages, lymphocytes, and eosinophils) and erythrocyte parameters (RBC, HGB, MCV, PLT and MPV) via a hemocytometer; and serum biochemical testing for tissue injury markers (AST, ALT, ALB, CRP, UREA, Crea, CK, and LDH) by biochemical analyzer.

Statistical analysis

Data are presented as mean ± standard error of the mean (SEM). Statistical analyses were performed using GraphPad Prism 9.5.0. Comparisons among multiple groups were performed using one-way analysis of variance (ANOVA). $P < 0.05$ was considered statistically significant.

Acknowledgement

We thank the Bioimaging Core Facilities and Multi-Omics Mass Spectrometry Core of Shenzhen Bay Laboratory for access to mass spectrometry and flow cytometry.

Funding Sources

The work is supported by Shenzhen Science and Technology Program KQTD20240729102213019.

References

1. Cullis, P.R.,Felgner, P.L. The 60-year evolution of lipid nanoparticles for nucleic acid delivery. *Nat. Rev. Drug Discov.* **23**, 709–722 (2024).
2. Liu, C., Shi, Q., Huang, X., Koo, S., Kong, N.,Tao, W. mRNA-based cancer therapeutics. *Nat. Rev. Cancer* **23**, 526–543 (2023).
3. Paunovska, K., Loughrey, D.,Dahlman, J.E. Drug delivery systems for RNA therapeutics. *Nat. Rev. Genet.* **23**, 265–280 (2022).
4. Mitchell, M.J., Billingsley, M.M., Haley, R.M., Wechsler, M.E., Peppas, N.A.,Langer, R. Engineering precision nanoparticles for drug delivery. *Nat. Rev. Drug Discov.* **20**, 101–124 (2021).
5. Hou, X., Zaks, T., Langer, R.,Dong, Y. Lipid nanoparticles for mRNA delivery. *Nat. Rev. Mater.* **6**, 1078–1094 (2021).
6. Albertsen, C.H., Kulkarni, J.A., Witzigmann, D., Lind, M., Petersson, K.,Simonsen, J.B. The role of lipid components in lipid nanoparticles for vaccines and gene therapy. *Adv. Drug Deliv. Rev.* **188** (2022).
7. Han, X., Zhang, H., Butowska, K., Swingle, K.L., Alameh, M.G., Weissman, D.,Mitchell, M.J. An ionizable lipid toolbox for RNA delivery. *Nat. Commun.* **12**, 7233 (2021).
8. Zhang, Y.B., Sun, C.Z., Wang, C., Jankovic, K.E.,Dong, Y.Z. Lipids and Lipid Derivatives for RNA Delivery. *Chem. Rev.* **121**, 12181–12277 (2021).
9. Parhiz, H., Brenner, J.S., Patel, P.N., Papp, T.E., Shahnawaz, H., Li, Q., Shi, R., Zamora, M.E., Yadegari, A., Marcos-Contreras, O.A., Natesan, A., Pardi, N., Shuvaev, V.V., Kiseleva, R., Myerson, J.W., Uhler, T., Riley, R.S., Han, X., Mitchell, M.J., Lam, K., Heyes, J., Weissman, D.,Muzykantov, V.R. Added to pre-existing inflammation, mRNA-lipid nanoparticles induce inflammation exacerbation (IE). *J. Control. Release* **344**, 50–61 (2022).
10. Moghimi, S.M.,Simberg, D. Pro-inflammatory concerns with lipid nanoparticles. *Mol. Ther.* **30**, 2109–2110 (2022).
11. Chen, S.P.,Blakney, A.K. Immune response to the components of lipid nanoparticles for ribonucleic acid therapeutics. *Curr. Opin. Biotechnol.* **85**, 103049 (2024).
12. Lee, Y., Jeong, M., Park, J., Jung, H.,Lee, H. Immunogenicity of lipid nanoparticles and its impact on the efficacy of mRNA vaccines and therapeutics. *Exp. Mol. Med*. **55**, 2085–2096 (2023).
13. Szebeni, J., Storm, G., Ljubimova, J.Y., Castells, M., Phillips, E.J., Turjeman, K., Barenholz, Y., Crommelin, D.J.A.,Dobrovolskaia, M.A. Applying lessons learned from nanomedicines to understand rare hypersensitivity reactions to mRNA-based SARS-CoV-2 vaccines. *Nat. Nanotechnol.* **17**, 337–346 (2022).
14. Sharma, P., Hoorn, D., Aitha, A., Breier, D.,Peer, D. The immunostimulatory nature of mRNA lipid nanoparticles. *Adv. Drug Deliv. Rev.* **205**, 115175 (2024).
15. Gustafson, H.H., Holt-Casper, D., Grainger, D.W.,Ghandehari, H. Nanoparticle Uptake: The Phagocyte Problem. *Nano Today* **10**, 487–510 (2015).
16. Lin, C., Kuzmanovic, A., Wang, N., Liao, L., Ernst, S., Penners, C., Jans, A., Hammoor, T., Stach, P.B., Peltzer, M., Volkert, I., Zechendorf, E., Hassan, R., Myllys, M., Liedtke, C., Herrmann, A., Chakraborty, G., Trautwein, C., Hengstler, J., Muller-Newen, G., Wang, J., Ghallab, A.,Bartneck, M. Exceptional Uptake, Limited Protein Expression: Liver Macrophages Lost in Translation of Synthetic mRNA. *Adv. Sci.* **12**, e2409729 (2025).
17. Manturthi, S., Courtemanche, A., Zaidi, Z., Patwari, A., Graham, L., Wang, L., Iqbal, U., Nguyen, T., Côté, M.,Gadde, S. Lipid Nanoparticles for Driving Macrophages to Promote Proinflammatory Cytokine Upregulation. *ACS Appl. Nano Mater.* **8**, 12818–12827 (2025).
18. Chaudhary, N., Kasiewicz, L.N., Newby, A.N., Arral, M.L., Yerneni, S.S., Melamed, J.R., LoPresti, S.T., Fein, K.C., Strelkova Petersen, D.M., Kumar, S., Purwar, R.,Whitehead, K.A. Amine headgroups in ionizable lipids drive immune responses to lipid nanoparticles by binding to the receptors TLR4 and CD1d. *Nat. Biomed. Eng.* **8**, 1483–1498 (2024).
19. MacMicking, J., Xie, Q.W.,Nathan, C. Nitric oxide and macrophage function. *Annu. Rev. Immunol.* **15**, 323–350 (1997).
20. Cinelli, M.A., Do, H.T., Miley, G.P.,Silverman, R.B. Inducible nitric oxide synthase: Regulation, structure, and inhibition. *Med. Res. Rev.* **40**, 158–189 (2020).
21. Minhas, R., Bansal, Y.,Bansal, G. Inducible nitric oxide synthase inhibitors: A comprehensive update. *Med. Res. Rev.* **40**, 823–855 (2020).
22. Wu, K.K., Xu, X., Wu, M., Li, X., Hoque, M., Li, G.H.Y., Lian, Q., Long, K., Zhou, T., Piao, H., Xu, A., Hui, H.X.,Cheng, K.K. MDM2 induces pro-inflammatory and glycolytic responses in M1 macrophages by integrating iNOS-nitric oxide and HIF-1alpha pathways in mice. *Nat. Commun.* **15**, 8624 (2024).
23. Kashfi, K., Kannikal, J.,Nath, N. Macrophage Reprogramming and Cancer Therapeutics: Role of iNOS-Derived NO. *Cells* **10** (2021).
24. Palmieri, E.M., Gonzalez-Cotto, M., Baseler, W.A., Davies, L.C., Ghesquiere, B., Maio, N., Rice, C.M., Rouault, T.A., Cassel, T., Higashi, R.M., Lane, A.N., Fan, T.W., Wink, D.A.,McVicar, D.W. Nitric oxide orchestrates metabolic rewiring in M1 macrophages by targeting aconitase 2 and pyruvate dehydrogenase. *Nat. Commun.* **11**, 698 (2020).
25. Theivendran, S., Gu, Z., Tang, J., Yang, Y., Song, H., Yang, Y., Zhang, M., Cheng, D.,Yu, C. Nanostructured Organosilica Nitric Oxide Donors Intrinsically Regulate Macrophage Polarization with Antitumor Effect. *ACS Nano* **16**, 10943–10957 (2022).
26. Mou, X., Shi, J., Zhang, W., Ma, Q., Wang, W., Huang, Y., Yin, S., Wang, Y., Huang, N., Pan, G., Yang, C.,Yang, Z. Mimicking Macrophage Immune Mechanism for Infection and Thrombosis Prevention on a Dual-Activity Hybrid Enzyme-Assembled Surface. *Angew. Chem. Int. Ed.* **65**, e19702 (2026).
27. Hu, X.L., Lv, X.Y., Wang, R., Long, H., Feng, J.H., Wang, B.L., Shen, W., Liu, H., Xiong, F., Zhang, X.Q., Ye, W.C.,Wang, H. Optimization of N-Phenylpropenoyl-l-amino Acids as Potent and Selective Inducible Nitric Oxide Synthase Inhibitors for Parkinson's Disease. *J. Med. Chem.* **64**, 7760–7777 (2021).

28. Li, W., Zheng, S., Higgins, M., Morra, R.P., Jr., Mendis, A.T., Chien, C.W., Ojima, I., Mierke, D.F., Dinkova-Kostova, A.T.,Honda, T. New Monocyclic, Bicyclic, and Tricyclic Ethynylcyanodienones as Activators of the Keap1/Nrf2/ARE Pathway and Inhibitors of Inducible Nitric Oxide Synthase. *J. Med. Chem.* **58**, 4738–4748 (2015).
29. Mukherjee, P., Cinelli, M.A., Kang, S.,Silverman, R.B. Development of nitric oxide synthase inhibitors for neurodegeneration and neuropathic pain. *Chem. Soc. Rev.* **43**, 6814–6838 (2014).
30. Yan, Y., Lu, A., Dou, Y., Zhang, Z., Wang, X.Y., Zhai, L., Ai, L.Y., Du, M.Z., Jiang, L.X., Zhu, Y.J., Shi, Y.J., Liu, X.Y., Jiang, D.,Wang, J.C. Nanomedicines Reprogram Synovial Macrophages by Scavenging Nitric Oxide and Silencing CA9 in Progressive Osteoarthritis. *Adv. Sci.* **10**, e2207490 (2023).
31. Herold, S., Mayer, K.,Lohmeyer, J. Acute lung injury: how macrophages orchestrate resolution of inflammation and tissue repair. *Front. Immunol.* **2**, 65 (2011).
32. Chen, X., Tang, J., Shuai, W., Meng, J., Feng, J.,Han, Z. Macrophage polarization and its role in the pathogenesis of acute lung injury/acute respiratory distress syndrome. *Inflamm. Res.* **69**, 883–895 (2020).
33. Fan, E.K.Y.,Fan, J. Regulation of alveolar macrophage death in acute lung inflammation. *Respir. Res.* **19**, 50 (2018).
34. Kang, M., Oh, J., Lee, C.,Lee, M. Emerging gene delivery nanosystems for the treatment of acute lung injury. *Nanomedicine (Lond)* **20**, 1881–1895 (2025).
35. Shin, H.E., Giannakopoulos, S., Park, J.D., Jang, H.J., Park, C.G., Murphy, S.V., Park, J., Verma, S.,Park, W. Lipid nanoparticles target neutrophils to reduce SARS-CoV-2-induced lung injury and inflammation. *J. Control. Release* **382**, 113736 (2025).
36. Sun, H., Zhang, Y., Wang, J., Su, J., Zhou, D., Yu, X., Xu, Y.,Yang, W. Application of Lung-Targeted Lipid Nanoparticle-delivered mRNA of soluble PD-L1 via SORT Technology in Acute Respiratory Distress Syndrome. *Theranostics* **13**, 4974–4992 (2023).
37. Zhao, G., Xue, L., Geisler, H.C., Xu, J., Li, X., Mitchell, M.J.,Vaughan, A.E. Precision treatment of viral pneumonia through macrophage-targeted lipid nanoparticle delivery. *Proc. Natl. Acad. Sci. U. S. A.* **121**, e2314747121 (2024).
38. Wang, Y., Liu, X., Xuan, W., Huang, W., Zhu, Y., Mao, C.,Liu, Y. Inhalable lipid nanoparticles for macrophage-specific STING gene editing to ameliorate pulmonary fibrosis. *Mol. Ther.* (2026).
39. Meng, Q., Popoola, D.O., Wang, C., Men, Y., Song, Y., Cao, Z., Novak, A., Li, Y.,Cooney, R.N. Lung-targeting lipid nanoparticle-mediated sparstolonin B delivery improves acute lung injury. *Biomater. Sci.* **13**, 5429–5441 (2025).
40. Wang, Q., Achour, J., Emam, L., Louaguenouni, Y., Cailleau, C., Mercier-Nome, F., Domenichini, S., Delomenie, C., Gul, S., Vergnaud, J., Tsapis, N., Mansart, A., Annane, D., Fay, F.,Fattal, E. Pulmonary Delivery of siRNA Anti-TNFalpha-loaded Lipid Nanoparticles for Rapid Recovery in Murine Acute Lung Injury. *Adv. Healthc. Mater.* **14**, e00695 (2025).
41. Zhao, Z., Shan, X., Ding, J., Ma, B., Li, B., Huang, W., Yang, Q., Fang, Y., Chen, J., Song, C., Wei, C., Liu, S., Cheng, X., Zhang, S., Liu, Y., Wu, H., Luo, C., Shu, S., Qiao, X., Wang, Z., Lu, X.,Miao, L. Boosting RNA nanotherapeutics with V-ATPase activating non-inflammatory lipid nanoparticles to treat chronic lung injury. *Nat. Commun.* **16**, 6477 (2025).
42. Bitounis, D., Jacquinet, E., Rogers, M.A.,Amiji, M.M. Strategies to reduce the risks of mRNA drug and vaccine toxicity. *Nat. Rev. Drug Discov.* **23**, 281–300 (2024).
43. Patel, M.N., Tiwari, S., Wang, Y., O'Neill, S., Wu, J., Omo-Lamai, S., Espy, C., Chase, L.S., Majumder, A., Hoffman, E., Shah, A., Sarkozy, A., Katzen, J., Pardi, N.,Brenner, J.S. Safer non-viral DNA delivery using lipid nanoparticles loaded with endogenous anti-inflammatory lipids. *Nat. Biotechnol.* **44**, 79–89 (2026).
44. Zhang, H., Han, X., Alameh, M.G., Shepherd, S.J., Padilla, M.S., Xue, L., Butowska, K., Weissman, D.,Mitchell, M.J. Rational design of anti-inflammatory lipid nanoparticles for mRNA delivery. *J. Biomed. Mater. Res. A* **110**, 1101–1108 (2022).
45. Chen, K., Li, X., Feng, S., Li, Y., Jiang, T., Liu, Y., Guo, N., Zeng, X., Yao, H., Qiu, M., Lu, J.,Lin, J. Hydroxychloroquine-functionalized ionizable lipids mitigate inflammatory responses in mRNA therapeutics. *J. Control. Release* **387**, 114267 (2025).
46. Yi, G., Li, M., Zhou, J., Li, J., Song, X., Li, S., Liu, J., Zhang, H.,Chen, Z. Novel pH-responsive lipid nanoparticles deliver UA-mediated mitophagy and ferroptosis for osteoarthritis treatment. *Mater. Today Bio.* **32**, 101697 (2025).
47. Rananaware, P., Singh, S.,Brahmkhatri, V.P. Scavenging of reactive oxygen and nitrogen species using nanoparticles and their applications in disease management. *RSC Adv.* **15**, 47955–47980 (2025).
48. Pan, L., Zhang, L., Deng, W., Lou, J., Gao, X., Lou, X., Liu, Y., Yao, X., Sheng, Y., Yan, Y., Ni, C., Wang, M., Tian, C., Wang, F.,Qin, Z. Spleen-selective co-delivery of mRNA and TLR4 agonist-loaded LNPs for synergistic immunostimulation and Th1 immune responses. *J. Control. Release* **357**, 133–148 (2023).
49. Espy, C.L., Wu, J., Omo-Lamai, S., Wang, L., Dong, F., Milosavljevic, A., O'Neill, S., Brysgel, T., Wang, Y., Zaleski, M., Wolfe, E., Maheshwari, R., Patel, M., Trauner, D., Nong, J., Wang, Z.,Brenner, J.S. Localized NF-kappaB Inhibition Reduces Lipid Nanoparticle-Associated Inflammation. *Adv. Sci.* e17931 (2026).
50. Frohlich, E. The role of surface charge in cellular uptake and cytotoxicity of medical nanoparticles. *Int. J. Nanomedicine* **7**, 5577–5591 (2012).
51. Kedmi, R., Ben-Arie, N.,Peer, D. The systemic toxicity of positively charged lipid nanoparticles and the role of Toll-like receptor 4 in immune activation. *Biomaterials* **31**, 6867–6875 (2010).
52. Cui, S., Wang, Y., Gong, Y., Lin, X., Zhao, Y., Zhi, D., Zhou, Q.,Zhang, S. Correlation of the cytotoxic effects of cationic lipids with their headgroups. *Toxicol. Res.* **7**, 473–479 (2018).
53. Vanucci-Bacque, C.,Bedos-Belval, F. Anti-inflammatory activity of naturally occuring diarylheptanoids - A review. *Bioorg. Med. Chem.* **31**, 115971 (2021).
54. Rath, M., Muller, I., Kropf, P., Closs, E.I.,Munder, M. Metabolism via Arginase or Nitric Oxide Synthase: Two Competing Arginine Pathways in Macrophages. *Front. Immunol.* **5**, 532 (2014).
55. Thomas, A.C.,Mattila, J.T. "Of mice and men": arginine metabolism in macrophages. *Front. Immunol.* **5**, 479 (2014).
56. Zhang, H., Liu, D., Yang, K., Liang, Z.,Li, M. Ionizable guanidine-based lipid nanoparticle for targeted mRNA delivery and cancer immunotherapy. *Sci. Adv.* **11**, eadx5970 (2025).
57. Hwang, T.L., Aljuffali, I.A., Lin, C.F., Chang, Y.T.,Fang, J.Y. Cationic additives in nanosystems activate cytotoxicity and inflammatory response of human neutrophils: lipid nanoparticles versus polymeric nanoparticles. *Int. J. Nanomedicine* **10**, 371–385 (2015).
58. Ndeupen, S., Qin, Z., Jacobsen, S., Bouteau, A., Estanbouli, H.,Igyarto, B.Z. The mRNA-LNP platform's lipid nanoparticle component used in preclinical vaccine studies is highly inflammatory. *iScience* **24**, 103479 (2021).